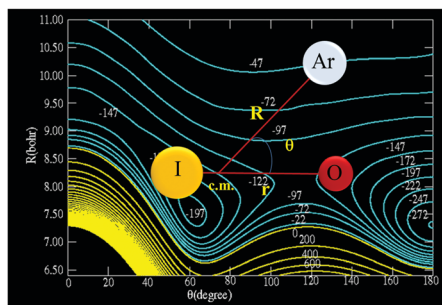# Physical Chemistry Chemical Physics

c9cp05310g

We have presented the Graphical Abstract text and image for your article below. This brief summary of your work will appear in the contents pages of the issue in which your article appears.

IO(X²Π)−Ar cluster: *ab initio* potential energy surface and dynamical computations

Q2

S. Marzouk, Y. Ajili, F. Lique, M. Ben El Hadj Rhouma, M. Mogren Al Mogren and M. Hochlaf*

Iodine oxide (IO) is an important tropospheric molecule.

Q3

Please check this proof carefully. Our staff will not read it in detail after you have returned it.

Please send your corrections either as a copy of the proof PDF with electronic notes attached or as a list of corrections. **Do not edit the text within the PDF or send a revised manuscript** as we will not be able to apply your corrections. Corrections at this stage should be minor and not involve extensive changes.

Proof corrections must be returned as a single set of corrections, approved by all co-authors. No further corrections can be made after you have submitted your proof corrections as we will publish your article online as soon as possible after they are received.

Please ensure that:
- The spelling and format of all author names and affiliations are checked carefully. You can check how we have identified the authors' first and last names in the researcher information table on the next page. **Names will be indexed and cited as shown on the proof, so these must be correct.**
- Any funding bodies have been acknowledged appropriately and included both in the paper and in the funder information table on the next page.
- All of the editor's queries are answered.
- Any necessary attachments, such as updated images or ESI files, are provided.

Translation errors can occur during conversion to typesetting systems so you need to read the whole proof. In particular please check tables, equations, numerical data, figures and graphics, and references carefully.

Please return your **final** corrections, where possible within **48 hours** of receipt, by e-mail to: pccp@rsc.org. If you require more time, please notify us by email.

Funding information

Providing accurate funding information will enable us to help you comply with your funders' reporting mandates. Clear acknowledgement of funder support is an important consideration in funding evaluation and can increase your chances of securing funding in the future.

We work closely with Crossref to make your research discoverable through the Funding Data search tool (http://search.crossref.org/funding). Funding Data provides a reliable way to track the impact of the work that funders support. Accurate funder information will also help us (i) identify articles that are mandated to be deposited in **PubMed Central (PMC)** and deposit these on your behalf, and (ii) identify articles funded as part of the **CHORUS** initiative and display the Accepted Manuscript on our web site after an embargo period of 12 months.

Further information can be found on our webpage (http://rsc.li/funding-info).

What we do with funding information

We have combined the information you gave us on submission with the information in your acknowledgements. This will help ensure the funding information is as complete as possible and matches funders listed in the Crossref Funder Registry.

If a funding organisation you included in your acknowledgements or on submission of your article is not currently listed in the registry it will not appear in the table on this page. We can only deposit data if funders are already listed in the Crossref Funder Registry, but we will pass all funding information on to Crossref so that additional funders can be included in future.

Please check your funding information

The table below contains the information we will share with Crossref so that your article can be found *via* the Funding Data search tool. **Please check that the funder names and grant numbers in the table are correct and indicate if any changes are necessary to the Acknowledgements text.**

Funder name	Funder's main country of origin	Funder ID (for RSC use only)	Award/grant number
King Saud University	Saudi Arabia	501100002383	RGP-333
Centre National de la Recherche Scientifique	France	501100004794	Unassigned
Centre National d'Etudes Spatiales	France	501100002830	Unassigned

Q1

Researcher information

Please check that the researcher information in the table below is correct, including the spelling and formatting of all author names, and that the authors' first, middle and last names have been correctly identified. **Names will be indexed and cited as shown on the proof, so these must be correct.**

If any authors have ORCID or ResearcherID details that are not listed below, please provide these with your proof corrections. Please ensure that the ORCID and ResearcherID details listed below have been assigned to the correct author. Authors should have their own unique ORCID iD and should not use another researcher's, as errors will delay publication.

Please also update your account on our online manuscript submission system to add your ORCID details, which will then be automatically included in all future submissions. See here for step-by-step instructions and more information on author identifiers.

First (given) and middle name(s)	Last (family) name(s)	ResearcherID	ORCID iD
S.	Marzouk		
Y.	Ajili		
F.	Lique		0000-0002-0664-2536
M.	Ben El Hadj Rhouma		
M. Mogren	Al Mogren		
M.	Hochlaf		0000-0002-4737-7978

Queries for the attention of the authors

Editor's queries are marked on your proof like this **Q1**, **Q2**, etc. and for your convenience line numbers are indicated like this 5, 10, 15, ...

Please ensure that all queries are answered when returning your proof corrections so that publication of your article is not delayed.

Query reference	Query	Remarks
Q1	Funder details have been incorporated in the funder table using information provided in the article text. Please check that the funder information in the table is correct.	
Q2	Please confirm that the spelling and format of all author names is correct. Names will be indexed and cited as shown on the proof, so these must be correct. No late corrections can be made.	
Q3	Please check that the inserted Graphical Abstract text is suitable. If you provide replacement text, please ensure that it is no longer than 250 characters (including spaces).	
Q4	Please indicate where ref. 40 should be cited in the text.	
Q5	Ref. 82: Please provide the year of publication.	

IO(X²Π)−Ar cluster: *ab initio* potential energy surface and dynamical computations†

Q2

S. Marzouk,[ab] Y. Ajili,[c] F. Lique, [ID] [d] M. Ben El Hadj Rhouma,[a] M. Mogren Al Mogren[e] and M. Hochlaf [ID] *[b]

Iodine oxide (IO) is an important tropospheric molecule. In the present paper, we mapped the potential energy surfaces (PESs) of the doubly degenerate IO(X²Π)−Ar van der Waals system using single- and double-excitation coupled cluster approaches with non-iterative perturbation treatment of triple excitations [RCCSD(T)] extrapolated to the complete basis set (CBS) limit. In addition to bent local minima, we identified a linear Ar−IO complex as a global minimum. Afterwards, we performed scattering calculations on these PESs, considering the non-zero spin−orbit contribution and the Renner−Teller effect. The integral cross-sections exhibit an oscillatory structure *vs.* the final rotational state, as already observed for the NO(X²Π)−Ar system. Moreover, computations reveal that the Ar−IO complex is stable toward dissociation into IO and Ar. Therefore, it can be found in the atmosphere and participates in iodine compound physical chemical processes occurring there.

I. Introduction

The biogeochemical cycle of iodine is based on intense exchanges from the oceanic compartment to the atmosphere.[1] Iodine emissions to the atmosphere consist of iodine containing organic compounds, including methyl iodide (CH$_3$I),[2,3] a gas emitted abundantly in the ocean by the phytoplankton, hypoiodous acid (HIO)[4] and molecular iodine (I$_2$).[2–4] Once in the atmosphere, these volatile iodine compounds and the molecular iodine undergo dissociation processes by photolysis producing radicals, such as atomic I. These radicals are involved in a complex atmospheric chemistry leading, by reaction with ozone, to the formation of oxidized species (IO, I$_2$O, OIO...). These oxidized species then participate in the formation of aerosols and condensation of clouds and they are strongly suspected to be involved in the ozone destruction over the oceans.[5–8] In particular, tropospheric IO can be formed *via* the reaction I + O$_3$ → IO + O$_2$. It thus participates directly in the photochemical ozone loss in the tropical Atlantic Ocean boundary layer. It can also impact indirectly the ozone

budget in the atmosphere *via* its implication in the photochemistry of tropospheric HO$_x$ and NO$_x$ (production/destruction).

Several details on IO spectroscopy and its gas phase reactivity can be found in ref. 9 and 10. For instance, the kinetics and mechanisms of reactions involving the IO molecule have been studied in a large number of laboratory studies.[11–19] Experimental data on the thermochemistry of the IO molecule are also available.[20] Moreover, the physical properties of the isolated molecule are also available.[21–24] Its spectroscopy was investigated by a multitude of experimental and theoretical[25–29] approaches. These include μw,[21] rotational,[30] laser magnetic resonance,[31] cavity ring-down,[32] high-resolution laser-rf,[33] laser induced fluorescence[11,12] and absorption and emission spectroscopies[34–36] as well as spin−orbit configuration interaction calculations.[37–39] These studies established that the ground state of IO is of ²Π symmetry species.[33] It is a Hund's case (a) radical with a negative spin−orbit constant (A_{SO} = −2091 cm^{-1} [22]). The electronic orbital angular momentum and the electron spin have well-defined projection onto the internuclear axis of $\Lambda = \pm 1$ and $\Sigma = \pm 1/2$, respectively. Therefore, there are two spin−orbit manifolds: the lowest component is the ²Π$_{3/2}$ with $|\Omega| = |\Lambda + \Sigma| = 3/2$ (labeled F$_1$), and the higher-energy is the ²Π$_{1/2}$ with $|\Omega| = 1/2$ (labeled F$_2$). Each rotational j splits into two close lying Λ-doublet levels labeled e (total parity + as $(-1)^{j-1/2}$) and f (total parity − as $(-1)^{j-1/2}$).[42] The energies of the rotational levels, including the spin−orbit and Λ-doubling fine structure, are given by:

$$E_{j,\Omega=1/2,\varepsilon} = 1/2 A_{SO} + B_e[j(j+1) + 1/4] + \frac{\varepsilon}{2}p(j+1/2) \quad (1)$$

^{a} *Laboratoire de Recherche d'Etude des Milieux Ionisés et Réactifs (EMIR), Institut Préparatoire aux Etudes d'Ingénieurs de Monastir, Université de Monastir, Tunisia*
^{b} *Université Gustave Eiffel, COSYS/LISIS, 5 Bd Descartes 77454, Champs sur Marne, France. E-mail: hochlaf@univ-mlv.fr; Fax: +33 1 60 95 73 20; Tel: +33 1 60 95 73 19*
^{c} *Laboratoire de Spectroscopie Atomique, Moléculaire et Applications – LSAMA, Université de Tunis-El Manar, Tunis, Tunisia*
^{d} *LOMC – UMR 6294, CNRS-Université du Havre, 25 rue Philippe Lebon, BP 1123, 76 063 Le Havre Cedex, France*
^{e} *King Saud University, Department of Chemistry, Faculty of Science, PO Box 2455, Riyadh 11451, Kingdom of Saudi Arabia*

† Electronic supplementary information (ESI) available. See DOI: 10.1039/c9cp05310g

This journal is © the Owner Societies 2019

Phys. Chem. Chem. Phys., 2019, **00**, 1–8 | 1

$$E_{j,\Omega=3/2,\varepsilon} = -1/2A_{SO} + B_e[j(j+1) - 7/4] + \frac{\varepsilon B_e}{2A_{SO}}$$

$$\times \left(2q + \frac{pB_e}{A_{SO}}\right)(j-1/2)(j+1/2)(j+3/2) \quad (2)$$

where ε is the parity. $\varepsilon = +1$ and $\varepsilon = -1$ correspond to e-labelled and f-labelled levels respectively. B_e (=0.3388 cm^{-1} [33]) is the rotational constant at equilibrium of IO (X$^2\Pi_{3/2}$). p (=0.1094212 cm^{-1} [30]) and q (=−0.0000166 cm^{-1} [30]) are the two Λ-doubling parameters (see ref. 30 for more details).

The present contribution deals with the investigation of the IO–Ar van der Waals complex. Ar is the third most abundant gas of the Earth's atmosphere. This complex may be formed in the troposphere/low stratosphere after collision between IO and argon. These collisional processes may participate in the modification of the radiation budget of the atmosphere. The implication in atmospheric processes of other IO–M complexes was noticed. For instance, the formation of the IO–water complex was suspected to be at the origin of the inhibition of the polymerization of IO leading to the atmospheric IO aerosols.[41] The existence of a stable IO–water complex was confirmed later by *ab initio* computations.[42] Also, the implication of the IO–CO van der Waals complex was suggested during the oxidation of IO by CO to form I + CO$_2$.[43] In the other hand, molecules containing iodine are prototype molecular systems for fundamental photophysical studies (see, for instance, the studies by Zewail and co-workers[44]). This is also true for the specific case of iodine van der Waals complexes such as those studied by Bogomolov *et al.*[45]

To date, nothing is available in the literature concerning the IO–Ar molecular species that may help its identification or elucidating its possible role in the physical chemical atmospheric phenomena. At present, we predict a stable IO–Ar complex. We derived its dissociation energy, which may help its identification in the laboratory. For that purpose, we generated the 2D potential energy surfaces (2D PESs) of the IO(X$^2\Pi$)–Ar interacting system. These PESs are mapped in the Jacobi coordinates (Fig. 1) using the coupled cluster approach extrapolated to the complete basis set (CBS) limit. Afterwards, these PESs are incorporated into full quantum treatment of the nuclear motions. Because of the $^2\Pi$ nature of IO, the ground state of the IO–Ar complex is doubly degenerate for linear configurations with non-zero spin–orbit contribution. This results in a Renner–Teller system,[46] which complicates the dynamics of such colliding systems. Such treatments are
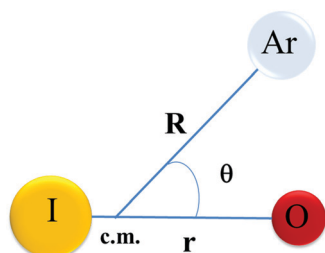
challenging and rare. For instance, we can cite the spectroscopic and dynamical investigations of the OH/OD–Rg (Rg = He, Ne, Ar, Kr, Xe),[47–53] PO–He,[54] NO–Rg (Rg = He, Ne, Ar),[55–67] NO–D$_2$,[60] and SH/SD–Ar[68] colliding systems.

II. Generation of the PESs of the IO (X$^2\Pi$)−Ar interacting system

1. Electronic structure computations

The IO–Ar van der Waals system is described using the Jacobi coordinates as specified in Fig. 1. They correspond to the IO internuclear distance (r), the distance from the center of mass of the IO molecule to the Ar atom (R) and the angle between R and the IO bond axis (θ), with $\theta = 0°$ for the collinear I–O–Ar arrangement. In the present study, the IO diatomic is considered as rigid. The IO bond distance was kept fixed at its experimental equilibrium value (r = 1.872 Å = 3.538 Bohr).[33] All electronic calculations were performed using the MOLPRO 2015 package[69] in the C_s symmetry point group.

When the IO(X$^2\Pi$) radical interacts with a spherical structure-less target (such as the Ar atom), the doubly-degenerate $^2\Pi$ electronic state splits into two components: one of $^2A'$ symmetry and one of $^2A''$ symmetry. *Ab initio* calculations of the PESs of Ar–IO(X$^2\Pi$) van der Waals complex being in the $^2A'$ or the $^2A''$ electronic states were carried out using the partially spin-restricted coupled clusters with the single, double and perturbative triple excitations (RCCSD(T))[70,71] approach as implemented in the MOLPRO 2015 package.[69] For both components, the electronic structure computations were carried out for θ angle values from $0°$ to $180°$ by steps of $10°$. The R distances were varied from 6 to 22 Bohr yielding 30 points for each angular orientation. Nevertheless, for $R > 14$ Bohr, some irregular behaviors were noticed. Thus, only the points where $R \leq 14$ Bohr were considered during the fitting of the PESs. For $R > 14$, the PESs were extrapolated (*cf. infra*).

For oxygen and argon atoms, we used the aug-cc-pVXZ (X = D, T, Q) basis sets of Dunning and co-workers.[72,73] The iodine was described using the corresponding aug-cc-pVXZ-PP (X = D, T, Q) correlation consistent basis sets together with the appropriate Stuttgart/Koeln ECP28MDF pseudopotential.[38] Throughout the calculations of the IO–Ar interaction potentials, $V(R,\theta)$, the basis set superposition error (BSSE) was corrected at all geometries using the Boys and Bernardi[74] counterpoise scheme, as follows

$$V(R,\theta) = E_{IO–Ar}(R,\theta) - E_{IO}(R,\theta) - E_{Ar}(R,\theta) \quad (3)$$

where the energies of the IO and Ar monomers are computed in the full basis set of the complex.

Afterwards, the *ab initio* energies were extrapolated to the Complete Basis Set (CBS) limit, employing the mixed exponential and Gaussian formula of Peterson *et al.*[75]

$$E = E_{CBS} + Ae^{-(X-1)} + Be^{-(X-1)^2} \quad (4)$$

Fig. 1 Definition of the Jacobi coordinates of the IO−Ar complex.

2 | *Phys. Chem. Chem. Phys.*, 2019, **00**, 1–8

This journal is © the Owner Societies 2019

where X is the basis set cardinal. $X = 2$, 3 and 4. E_{CBS} is the energy extrapolated to the CBS limit. A and B are parameters to adjust. In the following, we will discuss the RCCSD(T)/CBS PESs.

2. Analytic forms of the 2D-PESs

For the representation of the IO–Ar $^2A'$ and $^2A''$ 2D-PESs, we derived analytical expressions. We thus adopted the fitting procedure described by Werner et $al.$[76] for the CN–He complex. Such a procedure leads us to generate the $V(R,\theta)$ numerical expansion routine for each component:

$$V(R,\theta) = \sum_{l=1}^{L} A_l(R) d_{m,0}^{l+m-1}(\cos\theta) \tag{5}$$

where the $d_{m,0}^{l+m-1}$ are the reduced rotation matrix elements of Wigner and L represents the total number of the ab $initio$ angles. The $A_l(R)$ are given by

$$A_l(R) = e^{-a_l\left(R-R_l^{(0)}\right)}\left(\sum_{i=0}^{2} b_l^{(i)} R_i\right) - \frac{1}{2}\left(1 + \tanh\frac{R - R_l^{(1)}}{R_l^{Ref}}\right)\sum_{j=6,8,10} \frac{c_l^{(j)}}{R^j} \tag{6}$$

The analytic potentials were found to reproduce the calculated energies quite well. Over the entire grid, the mean difference between the analytic fit and the ab $initio$ computed interaction energies is less than 2–3%. The major deviations between the fitted potential values and the ab $initio$ points are concentrated in the long-range part of the PESs. The long-range part of the PES was extrapolated assuming a C_n/R^n ($n = 6, 8, 10$) multipolar expansion. The C_n coefficients were obtained from the ab $initio$ energies computed for distances larger than $R = 12$ a_0. The corresponding expansions are given in the ESI.†

In the scattering calculations, it is more convenient to use the average and the difference of the $V_{A'}$ and $V_{A''}$ potential energy surfaces which we define as:

$$V_{sum} = 1/2\left(V_{A''} + V_{A'}\right) \tag{7}$$

$$V_{diff} = 1/2\left(V_{A''} - V_{A'}\right) \tag{8}$$

These two adiabatic potentials are usually expanded in a series of reduced Wigner functions $d_\mu(\cos\theta)$,[77]

$$V_{sum}(R,\theta) = \sum_{l=0}^{l_{max}} V_{l0}(R) d_{l0}(\cos\theta) \tag{9}$$

$$V_{diff}(R,\theta) = \sum_{l=0}^{l_{max}} V_{l2}(R) d_{l2}(\cos\theta) \tag{10}$$

where $V_{l0}(R)$ and $V_{l2}(R)$ correspond to the radial dependence of the potentials as expressed in ref. 77. l_{max} was set to 18.

In the pure Hund's case (a), V_{sum} is responsible for inducing inelastic collisions within a given spin manifold, and V_{diff} for inducing inelastic collisions between the $^2\Pi_{1/2}$ and $^2\Pi_{3/2}$ spin–orbit manifolds.

3. Features of the $^2A'$ and $^2A''$ 2D-PESs

Fig. 2 shows the 2D contour plots of the $^2A'$ and $^2A''$ PESs along the R and θ Jacobi coordinates. Table 1 gives the main characteristics of these PESs including the geometric parameters of the stationary points, their well depths and isomerization barrier heights. Fig. 3 shows the minimum energy paths of the $^2A'$ ($V_{A'}$) and $^2A''$ ($V_{A''}$) components along the bending angle. For linear configurations, both components are degenerate and then split for bent structures. They form hence a linear–linear Renner–Teller system for $\theta = 180°$ and a linear–bent Renner–Teller system for $\theta = 0°$.[46] For both components, the global minimum occurs at a linear configuration, where the Ar is located at the iodine side of IO ($i.e.$ $\theta = 180°$) and for $R = 7.31$ Bohr. The associated well depth is $D_e = 273.58$ cm^{-1}. For the $^2A'$ state, we found a second local minimum for bent structures ($\theta = 56°$, $R = 7.67$ Bohr) with a well depth of $D_e = 197.90$ cm^{-1}. This minimum correlates with a transition state for $\theta = 0°$ and is separated by a transition state with the global minimum located at $\theta = 107°$ and $R = 7.94$ Bohr (Table 1). For the $^2A''$ state, two secondary minima are found: (i) at bent structures $i.e.$ $R = 7.46$ Bohr, $\theta = 63°$, $D_e = 217.49$ cm^{-1}; and (ii) at a linear Ar–
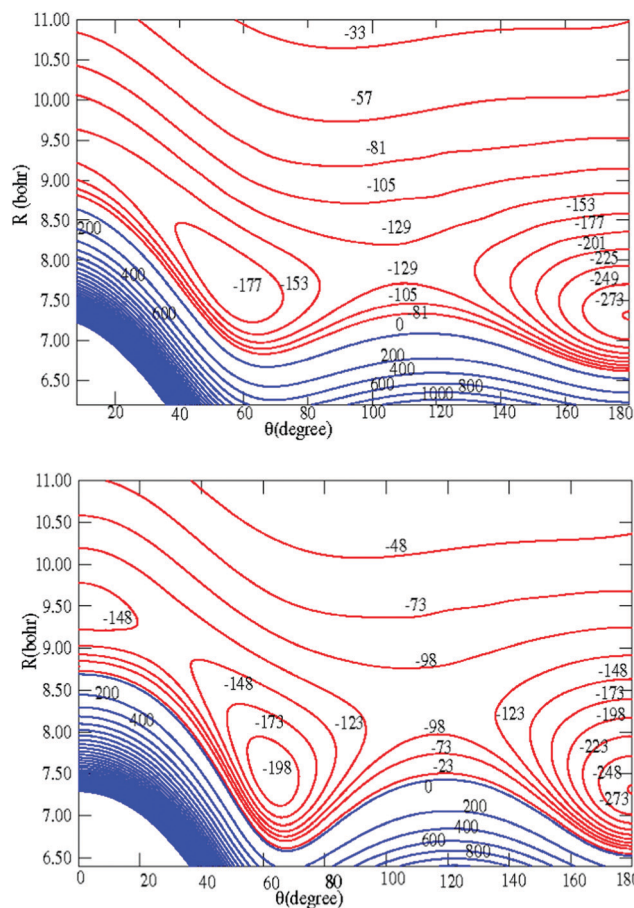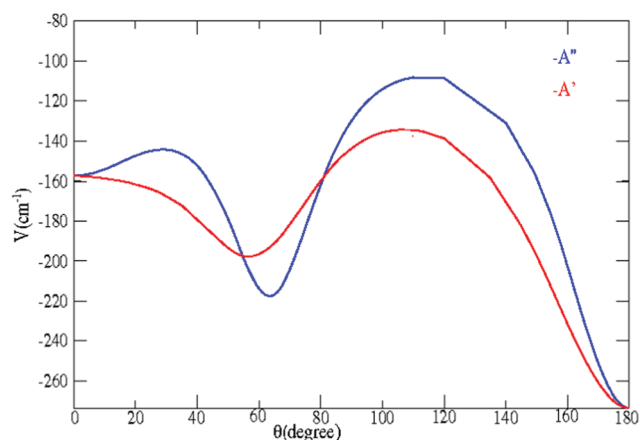

Fig. 2   2D contour plots of the $^2A'$ (top) and $^2A''$ (bottom) PESs of the IO–Ar complex. The blue (red) contours are for positive (negative) energies. Energies are in cm^{-1}. The reference energy is the energy at separated IO and Ar species.

Table 1 Characteristics of the IO–Ar PESs. We give the well depths (D_e, in cm^{-1}), equilibrium distances (R, in Bohr) and angles (θ in degrees) and the energies of the transition state (E^* in cm^{-1}) with respect to the IO and Ar separated species

$^2A''$ component

Ar–IO			Transition state			Bent IO–Ar			Transition state			IO–Ar		
D_e	R	θ	E^*	R	θ	D_e	R	θ	E^*	R	θ	D_e	R	θ
273.58	7.31	180°	−107.55	8.32	114	217.49	7.46	63°	−144.31	9.08	29	157.52	9.46	0°

$^2A'$ component

| Ar–IO			Transition state			Bent IO–Ar		
D_e	R	θ	E^*	R	θ	D_e	R	θ
273.58	7.31	180°	−134.42	7.94	107°	197.90	7.67	56°

Fig. 3 Minimum energy paths of the $^2A'$ ($V_{A'}$) and $^2A''$ ($V_{A''}$) components of the IO–Ar PES as a function of the θ angle.

O–I configuration *i.e.* $R = 9.46$, $\theta = 0°$, $D_e = 157.52$ cm^{-1}. As for the $^2A'$ component, the transition states connecting these minima are located below the dissociation of the complex (*cf.* Table 1). As discussed for other weakly bound complexes, complex quantum effects, including quantum tunneling, vibrational memory and quantum localization effects are expected to take place.[78,79] These effects together with the Renner–Teller coupling complicate the spectroscopy and the dynamics of the IO–Ar colliding system. Note that the features described here for the $^2A''$ PES are similar to those found for other van der Waals complexes such as ICl–Ar[80] and HI–Ar.[81]

4. Features of the V_{sum} and V_{diff} 2D-PESs

Fig. 4 presents the 2D contour plots of the V_{sum} and V_{diff}. As can be seen there, the average potential V_{sum} has two minima: (i) for the linear configuration, where $\theta = 180°$ and $R = 7.31$ cm^{-1} Bohr and $V_{sum} = -272.8$ cm^{-1}; and (ii) for the bent structure, where $\theta = 62°$ and $R = 7.52$ cm^{-1} Bohr and $V_{sum} = -204.7$ cm^{-1}; whereas $\theta = 0°$ corresponds to a transition state. Fig. 4 shows also that V_{diff} exhibits small variations along the R and θ coordinates. Thus, inelastic collisions between the $^2\Pi_{1/2}$ and $^2\Pi_{3/2}$ spin–orbit manifolds are not expected to take place.
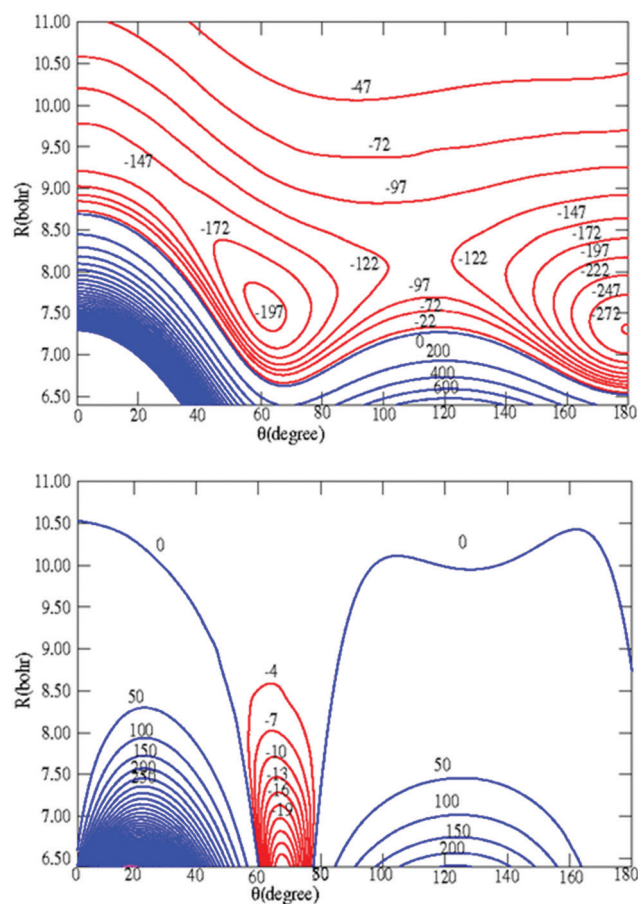
Fig. 4 2D contour plots of V_{sum} (top) and of V_{diff} (bottom) along the R and θ coordinates. The blue (red) contours are for positive (negative) energies. Energies are in cm^{-1}.

III. Dissociation energy of the IO–Ar complex

We carried out fully quantum close coupling calculations of the lowest bound states for total angular momentum $J = 0.5$, for the set of IO–Ar PESs determined here. In these calculations, the V_{sum} and V_{diff} were incorporated. The open-shell electronic

4 | *Phys. Chem. Chem. Phys.,* 2019, **00**, 1–8

This journal is © the Owner Societies 2019

structure of the IO molecule was taken into account. We employed the HIBRIDON suite of codes.[82]

The radial part of the wave functions in the bound-state calculations is expanded in a replicated Gaussian basis distributed between $R = 5.5$ and 20 Bohr. The IO–Ar reduced mass was 31.22 amu. The channel basis included all rotational levels of IO up to $j_{max} = 18.5$.

The calculated dissociation energy of IO–Ar, D_0, is ~ 228 cm^{-1}. Such a large value is explained by the relatively large well depth of both $^2A'$ and $^2A''$ PESs of the IO–Ar complex. This shows that the IO–Ar complex is expected to be stable under atmospheric conditions where it is also expected to be efficiently formed during collisions between IO and Ar.

IV. Integral cross-section calculations for the scattering of IO by collision with Ar

In the scattering calculations, we assume that the spin–orbit constant is independent of the IO–Ar intermolecular separation. The latter approximation is commonly employed in scattering calculations because of the moderate-to-large intermolecular separations at typical atmospheric collision energies. The quantum scattering calculations of integral cross-sections for the scattering of IO by collision with Ar were performed using the quantum Coupled States (CS) approximation.[83] We also performed some costly close coupling (CC) computations for comparison. Both techniques are implemented in the HIBRIDON package.[82]

The numerical accuracy of the integration procedure with respect to the number of partial waves and rotational basis functions and the integration parameters were tested to meet convergence criteria better than 2 percent for the cross-sections.

Using eqn (1) and (2), we give in Table 2 the energies of the first fine structure levels of IO. The dynamical calculations were performed on a grid of energies up to a total energy of $E_{tot} = 500$ cm^{-1}. The maximum values of the total angular momentum and of the IO rotational quantum number were $J = 330.5$ and $j = 44.5$, respectively. For a better description of the resonances, the energy steps were spanned as follow: 0.1 for $E_{tot} \leq 100$, 0.2 for $100 \leq E_{tot} \leq 200$, and 0.5 for $200 \leq E_{tot} \leq 300$ and 1 cm^{-1} for $E_{tot} \geq 300$ (all values are in cm^{-1}).

In order to check the accuracy of the CS approximation, a comparison with the exact close coupling (CC) approach has been carried out. Table 3 gives the comparison with the two methods for some transitions where the collision energy, E_{tot} is equal to 50 cm^{-1} and 300 cm^{-1}. As expected, the CS cross-sections differ significantly from those obtained using exact CC calculations at very low collision energies. This difference however vanishes while increasing the total energy. Indeed, Table 3 shows that the CS approach can lead to inaccuracies of 20–50 percent at total energy of 50 cm^{-1}, whereas the agreement improves significantly between CC and CS cross sections for $E_{tot} = 300$ cm^{-1}. The relative accuracy of the CS

Table 2 Pattern of the rotational levels (j) of IO (X$^2\Pi$) for $\Omega = 1/2$ and 3/2. Energies ($E_{\Omega=3/2}$ and $E_{\Omega=1/2}$) are in cm^{-1}. ε is the parity. The reference energy is that of the $E_{\Omega=3/2}$ $j = 1.5$ level

j	ε	$E_{\Omega=3/2}$	$E_{\Omega=1/2}$
0.5	e		2090.771
0.5	f		2090.661
1.5	e	0.000	2091.842
1.5	f	0.000	2091.623
2.5	e	1.694	2093.591
2.5	f	1.694	2093.263
3.5	e	4.065	2096.018
3.5	f	4.065	2095.580
4.5	e	7.113	2099.122
4.5	f	7.113	2098.575
5.5	e	10.839	2102.904
5.5	f	10.839	2102.248
6.5	e	15.243	2107.364
6.5	f	15.243	2106.598
7.5	e	20.324	2112.502
7.5	f	20.324	2111.626
8.5	e	26.082	2118.317
8.5	f	26.082	2117.332
9.5	e	32.518	2124.810
9.5	f	32.518	2123.716
10.5	e	39.631	2131.980
10.5	f	39.631	2130.777
11.5	e	47.422	2139.829
11.5	f	47.422	2138.516
12.5	e	55.890	2148.355
12.5	f	55.890	2146.933
13.5	e	65.036	2157.559
13.5	f	65.036	2156.027
14.5	e	74.859	2167.440
14.5	f	74.859	2165.799
15.5	e	85.359	2177.999
15.5	f	85.359	2176.249

Table 3 Comparison between CC and CS IO–Ar cross-sections (in Å) for total energies $E_{tot} = 50$ cm^{-1} and $E_{tot} = 300$ cm^{-1}. Transitions were chosen among levels in the F$_1$ spin–orbit manifold

Transition	$E_{tot} = 50$ cm^{-1}		$E_{tot} = 300$ cm^{-1}	
	CC	CS	CC	CS
1.5 e → 1.5 f	22.71	46.81	10.46	14.17
1.5 e → 3.5 e	7.130	4.808	2.786	3.136
1.5 e → 3.5 f	7.136	7.865	3.333	3.880
1.5 e → 4.5 e	5.386	4.830	2.170	2.187
1.5 e → 4.5 f	4.920	3.787	1.311	1.529
1.5 e → 5.5 e	4.644	3.323	0.978	0.936
1.5 e → 5.5 f	4.289	3.305	1.373	1.315
2.5 e → 6.5 e	6.623	6.191	1.297	1.137
2.5 e → 6.5 f	5.685	4.867	1.479	1.554
3.5 e → 8.5 e	4.849	7.023	1.579	1.389
4.5 e → 6.5 e	9.774	9.213	4.319	3.865
7.5 e → 10.5 e	15.64	12.39	3.549	4.123
10.5 e → 11.5 e	30.23	28.80	10.16	9.762
10.5 e → 15.5 e	—[a]	—[a]	2.435	2.610

[a] Energetically inaccessible transition.

approximation compared to the full CC approach can be explained by the relatively small energy spacing between IO rotational levels (Table 2).

As mentioned above, the IO molecule can be described in the Hund's case (a) with a large spin–orbit splitting (of 2091
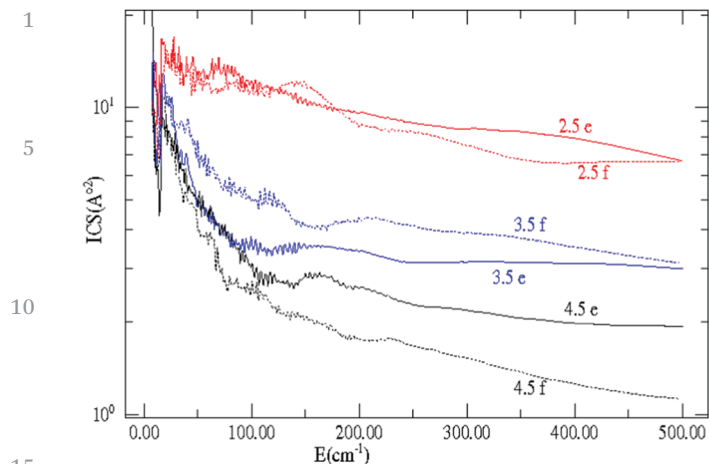
This journal is © the Owner Societies 2019

Phys. Chem. Chem. Phys., 2019, **00**, 1–8 | **5**

Fig. 5 Variation of the cross-sections *vs.* the collision energy for transitions out of the (j = 1.5, e, F_1) fine structure level to the (j', e/f, F_1) spin–orbit level manifold.

cm^{-1}) between Ω = 3/2 and Ω = 1/2 states. As expected, no spin–orbit changing transitions occur during the collisions between the Ω = 3/2 and Ω = 1/2 manifolds, which are induced by V_{diff}. Whereas V_{sum} potential, which is responsible for the collisional excitation within a given spin–orbit manifold, shows large variations (Fig. 4).

Fig. 5 displays the integral cross-sections of IO induced by collision with Ar as a function of the collision energy for transitions out of the rotational level (j = 1.5, e) of the F_1 spin–orbit manifold to some selected rotational levels (j', e/f) within the F_1 manifold. As may be seen, regardless of the transition considered, the cross-sections show a dense resonance structure at low energies (E < 200 cm^{-1}). They correspond to both shape resonances and Feshbach resonances resulting from the decay of bound and quasi-bound states supported by the IO–Ar weakly bound wells in the $^2A'$ and $^2A''$ potentials. It is clear also that the cross-sections for spin–orbit conserving transitions present a strong propensity in favor of the parity conserving e → e and with Δj = 1.
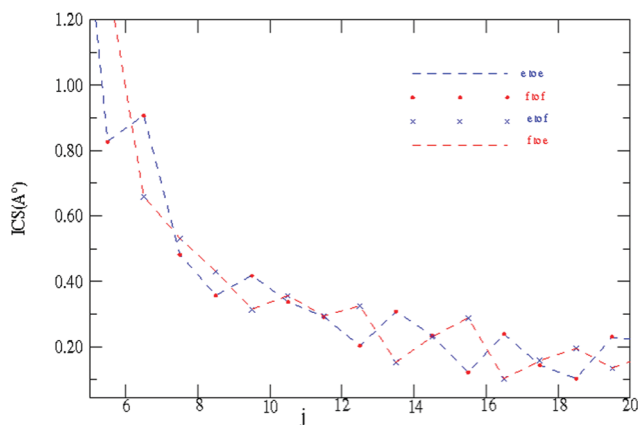
As explained by Dagdigian *et al.*,[84] the values of the integral cross sections for e → e and e → f collisions should be identical to those of f → f and f → e, respectively[84] in the limit case of a pure Hund's case (a). This is the case here. Indeed, these e/f conserving and changing cross-sections are illustrated in Fig. 6, which shows the integral cross sections obtained for IO($X^2\Pi$) colliding with Ar at E_{tot} = 500 cm^{-1} for spin–orbit conserving collisions, resolved into initial and final Λ-doublet levels. Fig. 6 shows also that the integral cross sections exhibit an oscillatory structure as a function of the final rotational state. This predicted alternation in the case of IO–Ar for the spin–orbit conserving transition was already noticed for the NO–Ar scattering system.[85]

V. Conclusions

We mapped the 2D PESs of the IO($X^2\Pi$)–Ar colliding system along the R and θ Jacobi coordinates. These PESs are incorporated later to treat the nuclear motions using quantum formalism. Computations show that the IO–Ar complex possesses a relatively large dissociation energy and thus it can be formed in the atmosphere. We also deduced the cross-sections of the excitation of IO colliding with Ar. Our calculations reveal that the integral cross sections present an oscillatory structure along the final rotational state. Such behavior was already noticed for the NO($X^2\Pi$)–Ar colliding system, for which several experimental and theoretical studies were devoted.

As said in the introduction, IO is playing an important role in the atmosphere. The present work should motivate new experimental investigations in the laboratory to characterize the IO ($X^2\Pi$)–Ar van der Waals system. Also, it should help in identifying this complex in the atmosphere and to understand the physical chemical processes involving IO there and more generally the iodine compounds.

Conflicts of interest

There are no conflicts to declare.

Acknowledgements

Fig. 6 Variation of the cross sections for the e → e, f → f, e → f and f → e transitions *vs.* the *j* quantum number.

6 | *Phys. Chem. Chem. Phys.*, 2019, **00**, 1–8

This journal is © the Owner Societies 2019

References

1   B. Alicke, K. Hebestreit, J. Stutz and U. Platt, *Nature*, 1999, **397**, 527.

2   W. L. Chameides and D. D. Davis, *J. Geophys. Res., B*, 1980, **85**, 7838.

3   W. Reifenhauser and K. G. Heuman, *Atmos. Environ., Part A*, 1992, **26**, 2905.

4   S. Klick and K. Abrahamson, *J. Geophys. Res.*, 1992, **97**, 12683.

5   L. J. Carpenter, *Chem. Rev.*, 2003, **103**, 4953–4962.

6   C. D. O'Dowd and T. Hoffmann, *Environ. Chem.*, 2005, **2**, 245–255.

7   S. Pechtl, E. R. Lovejoy, J. B. Burkholder and R. von Glasow, *Atmos. Chem. Phys.*, 2006, **6**, 505–523.

8   R. Vogt, R. Sander, R. V. Glasow and P. J. Crutzen, *J. Atmos. Chem.*, 1999, **32**, 375–395.

9   Y. Bedjanian and G. Poulet, *Chem. Rev.*, 2003, **103**, 4639.

10 A. Saiz-Lopez, J. M. C. Plane, A. R. Baker, L. J. Carpenter, R. von Glasow, J. C. Martín, G. McFiggans and R. W. Saunders, *Chem. Rev.*, 2012, **112**, 1773.

11 G. Inoue, M. Suzuki and N. Washida, *J. Chem. Phys.*, 1983, **79**, 4730.

12 A. A. Turnipseed, M. K. Gilles, J. B. Burkholder and A. R. Ravishankara, *Chem. Phys. Lett.*, 1995, **242**, 427.

13 M. K. Gilles, A. A. Turnipseed, J. B. Burkholder and A. R. Ravishankara, *Chem. Phys. Lett.*, 1997, **272**, 75.

14 M. H. Harwood, J. B. Burkholder, M. Hunter, R. W. Fox and A. R. Ravishankra, *J. Phys. Chem. A*, 1997, **101**, 853.

15 A. A. Turnipseed, M. K. Gilles., J. B. Burkholder and A. R. Ravishankara, *J. Phys. Chem. A*, 1997, **101**, 5517.

16 M. K. Gilles, A. A. Turnipseed, J. B. Burkholder, A. R. Ravishankara and S. Salomon, *J. Phys. Chem. A*, 1907, **101**, 5526.

17 Y. Bedjanian, G. Le Bras and G. Poulet, *J. Phys. Chem.*, 1996, **100**, 15130.

18 Y. Bedjanian, G. Le Bras and G. Poulet, *Chem. Phys. Lett.*, 1997, **266**, 233.

19 D. B. Atkinson, J. W. Hudgens and A. J. Orr-Ewing, *J. Phys. Chem.*, 1999, **103**, 6173.

20 M. W. Chase, *J. Phys. Chem. Ref. Data*, 1996, **25**, 1297.

21 S. Saito, *J. Mol. Spectrosc.*, 1973, **48**, 530.

22 M. K. Gilles, M. L. Polak and W. C. Lineberger, *J. Chem. Phys.*, 1991, **95**, 4723.

23 M. K. Gilles, M. L. Polak and W. C. Lineberger, *J. Chem. Phys.*, 1992, **96**, 8012.

24 Z. Zhang, P. S. Monks, L. J. Steif, J. F. Liebman, R. E. Huie, S. C. Kuo and R. B. Klemm, *J. Phys. Chem.*, 1996, **100**, 63–68.

25 C. Léonard, F. Le Quéré, P. Rosmus, C. Puzzarini and M. P. de Lara, Castells, *Phys. Chem. Chem. Phys.*, 2000, **2**, 1117.

26 B. Minaev, O. Loboda, O. Vahtras, H. Agren and E. Bilan, *Spectrochim. Acta, Part A*, 2002, **58A**, 1039.

27 P. Hassanzadeh and K. K. Irikura, *J. Phys. Chem. A*, 1997, **101**, 1580.

28 M. P. McGrath and F. S. Rowland, *J. Phys. Chem.*, 1996, **100**, 4815.

29 M. L. P. Rao, D. V. K. Rao and P. T. Rao, *Phys. Lett. A*, 1974, **50**, 341.

30 C. E. Miller and E. A. Cohen, *J. Chem. Phys.*, 2001, **115**, 6459.

31 F. Tamassia, S. M. Kermode and J. M. Brown, *J. Mol. Spectrosc.*, 2001, **205**, 92.

32 S. M. Newman, W. H. Howie, I. C. Lane, M. R. Upson and A. J. Orr-Ewing, *J. Chem. Soc., Faraday Trans.*, 1998, **94**, 2681.

33 J. P. Bekooy, W. L. Meerts and A. Dymanus, *J. Mol. Spectrosc.*, 1983, **102**, 320.

34 R. Stickel, A. Hynes, J. Bradshaw, W. Chameides and D. Davis, *J. Phys. Chem.*, 1988, **92**, 1862.

35 A. Loewenschuss, J. C. Miller and L. Andrews, *J. Mol. Spectrosc.*, 1980, **80**, 351.

36 T. Ingham, M. Cameron and J. N. Crowley, *J. Phys. Chem. A*, 2000, **104**, 8001.

37 S. Roszak, M. Krauss, A. B. Alekseyev, H.-P. Liebermann and R. J. Buenker, *J. Phys. Chem. A*, 2000, **104**, 2999.

38 K. A. Peterson, B. C. Shepler, D. Figgen and H. Stoll, *J. Phys. Chem. A*, 2006, **110**, 13877.

39 H. Hammami, O. Yazidi, M. B. E. H. Rhouma, M. M. A. Mogren and M. Hochlaf, *J. Chem. Phys.*, 2014, **141**, 014302.

40 J. M. Brown, J. T. Hougen, K.-P. Huber, J. W. C. Johns, I. Kopp, H. Lefebve-Brion, A. J. Merer, D. A. Ramsay, J. Rostas and R. N. Zare, *J. Mol. Spectrosc.*, 1975, **55**, 500. Q4

41 R. W. Saunders, A. S. Mahajan, J. C. Gómez Martín, R. Kumar and J. M. C. Plane, *Z. Phys. Chem.*, 2010, **224**, 1095–1117.

42 O. Gálvez, J. C. Gómez Martín, P. C. Gómez, A. Saiz-Lopez and L. F. Pacios, *Phys. Chem. Chem. Phys.*, 2013, **15**, 15572.

43 S. Khanniche, F. Louis, L. Cantrel and I. Cernusak, *J. Phys. Chem. A*, 2016, **120**, 1737–1749.

44 M. J. Rosker, M. Dantus and A. H. Zewail, *Science*, 1988, **241**, 1200–1202.

45 A. S. Bogomolov, V. G. Goldort, S. A. Kochubei and A. V. Baklanov, *J. Chem. Phys.*, 2017, **147**, 234304.

46 G. Herzberg, *Electronic Spectra and Electronic Structure of Polyatomic Molecules*, Van Nostrand, Toronto, ON, 1966.

47 Y. Kalugina, F. Lique and S. Marinakis, *Phys. Chem. Chem. Phys.*, 2014, **16**, 13500.

48 Y. Sumiyoshi, I. Funahara, K. Sato, Y. Ohshima and Y. Endo, *Phys. Chem. Chem. Phys.*, 2010, **12**, 8340.

49 Y. Sumiyoshi, I. Funahara, K. Sato, Y. Ohshima and Y. Endo, *Mol. Phys.*, 2010, **108**, 2207–2218.

50 Y. Sumiyoshi, I. Funahara, K. Sato, Y. Ohshima and Y. Endo, *J. Chem. Phys.*, 2006, **125**, 124307.

51 J. J. Gilijamse, S. Hoekstra, S. Y. T. van de Meerakker, G. C. Groenenboom and G. Meijer, *Science*, 2006, **313**, 1617.

52 L. Scharfenberg, K. B. Gubbels, M. Kirste, G. C. Groenenboom, A. van der Avoird, G. Meijer and S. Y. T. van de Meerakker, *Eur. Phys. J. D*, 2011, **65**, 189.

53 K. B. Gubbels, Q. Ma, M. Alexander, P. Dagdigian, D. Tanis, G. C. Groenenboom, A. van der Avoird and S. Y. T. van de Meerakker, *J. Chem. Phys.*, 2012, **136**, 144308.

54 F. Lique, I. Jiménez-Serra, S. Viti and S. Marinakis, *Phys. Chem. Chem. Phys.*, 2018, **20**, 5407.

55 Y. Sumiyoshi and Y. Endo, *J. Chem. Phys.*, 2017, **127**, 184309.

This journal is © the Owner Societies 2019

Phys. Chem. Chem. Phys., 2019, **00**, 1–8 | **7**

56 Z. Liu, W. Luo and C. Duan, *J. Chem. Phys.*, 2019, **150**, 064302.

57 V. Beutner, S. G. Zhang, H. Meyer and J. Kłos, *J. Chem. Phys.*, 2016, **145**, 124318.

58 J. Onvlee, S. N. Vogels, A. van der Avoird, G. C. Groenenboom and S. Y. T. van de Meerakker, *New J. Phys.*, 2015, **17**, 055019.

59 M. Brouard, H. Chadwick, C. J. Eyles, B. Hornung, B. Nichols, F. J. Aoiz, P. G. Jambrina, S. Stolte and M. P. de Miranda, *J. Chem. Phys.*, 2013, **138**, 104309.

60 H. Cybulski and B. Fernández, *J. Phys. Chem. A*, 2012, **116**, 7319–7328.

61 H. L. Holmes-Ross and W. D. Lawrance, *J. Chem. Phys.*, 2011, **135**, 014302.

62 J. C. Castro-Palacio, K. Ishii, J. Rubayo-Soneira and K. Yamashita, *Procedia Comput. Sci.*, 2011, **4**, 1135–1144.

63 S. N. Vogels, J. Onvlee, S. Chefdeville, A. van der Avoird, G. C. Groenenboom and S. Y. T. van de Meerakker, *Science*, 2015, **350**, 787.

64 A. von Zastrow, J. Onvlee, S. N. Vogels, G. C. Groenenboom, A. van der Avoird and S. Y. T. van de Meerakker, *Nat. Chem.*, 2016, **9**, 226.

65 J. Onvlee, A. van der Avoird, G. C. Groenenboom and S. Y. T. van de Meerakker, *J. Phys. Chem. A*, 2016, **120**, 4770.

66 T. de Jongh, T. Karman, S. N. Vogels, M. Besemer, J. Onvlee, A. G. Suits, J. O. F. Thompson, G. C. Groenenboom, A. van der Avoird and S. Y. T. van de Meerakker, *J. Chem. Phys.*, 2017, **147**, 013918.

67 J. Onvlee, S. N. Vogels, T. Karman, G. C. Groenenboom, S. Y. T. van de Meerakker and A. van der Avoird, *J. Chem. Phys.*, 2018, **149**, 084306.

68 Y. Sumiyoshi and Y. Endo, *J. Chem. Phys.*, 2005, **123**, 054325.

69 H.-J. Werner and P. J. Knowles, *et al.*, MOLPRO, version 2015.1, a package of ab initio programs, 2015, More details at http://www.molpro.net.

70 C. Hampel, K. A. Peterson and H.-J. Werner, *Chem. Phys. Lett.*, 1992, **190**, 1.

71 J. D. Watts, J. Gauss and R. J. Bartlett, *J. Chem. Phys.*, 1993, **98**, 8718.

72 T. H. Dunning, *J. Chem. Phys.*, 1989, **90**, 1007.

73 R. A. Kendall, T. H. Dunning and R. J. Harrison, *J. Chem. Phys.*, 1992, **96**, 6796.

74 S. F. Boys and F. Bernardi, *Mol. Phys.*, 1970, **19**, 553.

75 K. A. Peterson, D. E. Woon and T. H. Dunning, Jr., *J. Chem. Phys.*, 1994, **100**, 7410.

76 H.-J. Werner, B. Follmeg and M. H. Alexander, *J. Chem. Phys.*, 1988, **89**, 3139.

77 M. Alexander, *Chem. Phys.*, 1985, **92**, 337.

78 Y. Ajili, T. Trabelsi, O. Denis-Alpizar, T. Stoecklin, A. G. Csaszar, M. Mogren Al-Mogren, J. S. Francisco and M. Hochlaf, *Phys. Rev. A*, 2016, **93**, 052514.

79 M. Lara-Moreno, T. Stoecklin, P. Halvick and M. Hochlaf, *Phys. Chem. Chem. Phys.*, 2019, **21**, 3550.

80 A. Valdés, R. Prosmiti, P. Villarreal and G. Delgado-Barrio, *Chem. Phys. Lett.*, 2003, **357**, 328.

81 R. Prosmiti, S. Lopez-Lopez and A. Garcia-Vela, *J. Chem. Phys.*, 2004, **120**, 14.

82 M. H. Alexander, D. E. Manolopoulos, H.-J. Werner, B. Follmeg, and P. Dagdigian with contributions by D. Lemoine, P. F. Vohralik, G. Corey, R. Gordon, B. Johnson, T. Orlikowski, A. Berning, A. Degli-Esposti, C. Rist, B. Pouilly, J. Klos, Q. Ma, G. van der Sanden, M. Yang, F. de Weerd, S. Gregurick and F. Lique, The HIBRIDON package (version 4.4), http://www2.chem.umd.edu/groups/alexander/.

83 P. McGuire and D. J. Kouri, *J. Chem. Phys.*, 1974, **60**, 463.

84 P. J. Dagdigian, M. H. Alexander and K. P. Liu, *J. Chem. Phys.*, 1989, **91**, 839.

85 M. H. Alexander and S. Stolte, *J. Chem. Phys.*, 2000, **112**, 18.